Science of Sintering, **54** (2022) 335-347

https://doi.org/10.2298/SOS2203335P

UDK: 669.018; 622.785; 692.533.1

Superalloy/Al_2O_3 type Composite Compacts Obtained by Spark Plasma Sintering from Mechanically Alloyed Powders

Călin V. Pricăˣ⁾, Niculina A. Sechel, Bogdan V. Neamțu, Traian F. Marinca, Florin Popa, Horea F. Chicinaș, Ionel Chicinaș

Materials Science and Engineering Department, Technical University of Cluj-Napoca, 103-105, Muncii Avenue, 400641 Cluj-Napoca, Romania

Abstract:

Fe-base Superalloy/Al_2O_3 type composite compacts were successfully obtained by spark plasma sintering from mechanically alloyed powders. The superalloy powders without Al_2O_3 and superalloy/Al_2O_3 type composites powders with 5 and 10 %vol. Al_2O_3 were synthesized from elemental powders in a high energy planetary mill. The influence of the milling process on particle size evolution has been determined using a Laser Particle Size Analyzer with an analysis field of 0.1-1000 μm. The composite compacts were obtained by spark plasma sintering. Both, composite powders, and compacts were investigated by X-ray diffraction (XRD), high temperature X-ray diffraction (HT-XRD), scanning electron microscopy (SEM) and energy dispersive X-ray spectroscopy (EDX).

Keywords*: Superalloy/Al_2O_3 composite; Mechanical alloying; Spark plasma sintering.*

1. Introduction

Superalloys are part of the group of Ni, Ni-Co and Co base alloys and show- high oxidation resistance, hot corrosion properties, creep resistance and very good mechanical properties at high temperature [1-5]. Usually, superalloys can operate at a high fraction of their melting point. Because of this, superalloys are used in jet engine components such as turbine blades and combustion chamber [6]. Oxide Dispersion Strengthening (ODS) superalloys have been researched in the last decades because the ODS superalloys have excellent high-temperature creep-rupture strength and resistance oxidation and corrosion is higher than those of the superalloys [7,8]. Superalloy/Al_2O_3 type composites belong to the group of materials known as ceramic reinforced metal matrix composites (MMCs) [9-11]. The ceramic component offers high resistance to heat, wear, corrosion, and creep; the metal component provides thermal conductivity, toughness, and mechanical strength. An important parameter to ensure these properties of the composite is the particle sizes and dispersion of the ceramic component. A decrease in ceramic particle size and a homogeneous distribution leads to mechanical properties of MMCs increasing. Also, the ceramic particle prevents the crystallite size increasing at high temperatures with positive impact on mechanical properties.

One of the common methods to produce MMCs powders is the mechanical alloying (MA) process [12]. MA is a non-equilibrium process to obtain far from equilibrium structures, including amorphous alloy, metastable nanostructured phases, nanomaterials with extended solubility, intermetallic compounds and oxide dispersion strengthened alloys (ODS) [13-16]. This technique involves the high energy ball milling of metallic and oxide powders

ˣ⁾ **Corresponding author:** calin.prica@stm.utcluj.ro

to obtain a composite powder with a nanosized structure and a high degree of ceramic powder dispersion in metal matrix. The most used ceramic component in MMCs is Al_2O_3 powders due to their thermal stability [17-19]. Fe base superalloy are chosen as a metal matrix due to that their lower cost compared with the Ni and Co base superalloys.

Spark plasma sintering (SPS) is a new technique for rapid sintering of powders to obtained composite compacts [20-22]. By SPS the crystallite growth is limited, and the nanostructure result after MA process is maintained [20]. The SPS technology consists in a high temperature pressing of powders in a graphite die. Simultaneous a DC current pulses are involved. A plasma discharge between powder particle occurs which lead to their sintering [23-26]. This process has been widely used to obtain magnetic materials, ODS alloys and composite Fe, Ni and Co superalloy reinforced with ceramic particles [16,27,28]. In our previous study, we obtained the Al_2O_3/Ni composite, in which the alumina particles are uniformly dispersed in a quasi-continuously Ni network [29].

In this paper, we present the studies regarding the synthesis of the Superalloy/Al_2O_3 composite compacts by SPS from mechanically alloyed composite powders.

2. Materials and Experimental Procedures

The elemental Fe, Ni, Cr, Ti and B powders with purities over 99.5 % was used as raw materials for obtaining the Fe base superalloy powder with the nominal composition given in Table I. The powders particles size used in the experimental studies is as follows: -150 μm for iron, -10 μm for nickel, -250 μm for chrome, -88 μm for titanium and -40 μm for boron. To obtain the MMCs powders we added 5 and 10 %vol. Al_2O_3 with particle size -20 μm, as ceramic reinforcement. The compositions of samples are shown in Tables I and II.

Tab. I The composition of Fe base superalloy powders (starting samples).

Chemical composition, wt.%					
	Fe	Ni	Cr	Ti	B
FeCrNiTiB (Fe base Superalloy)	57.25	26	15	1.7	0.05

Tab. II MMCs powders composition (starting samples).

Samples	**Al_2O_3 (vol.%)**	**Theoretical density (g/cm^3)**
FeCrNiTiB	0	7.93
FeCrNiTiB+5 % Al_2O_3	5	7.73
FeCrNiTiB+10 % Al_2O_3	10	7.53

The powders were milled up to 16 h in a Fritsch Pulverisette 6 (high energy planetary ball mill), using a hardened steel vial and balls. The mechanical alloying process was carried out in an argon atmosphere to prevent sample oxidation. The ball to powder mass ratio – BPR was 10:1. The vial rotation speed was set at 300 rpm. Several milling times, ranging from 1 to 16 h has been chosen for collecting samples. The milled powders were then consolidated by spark plasma sintering (SPS) technique to obtain nanocrystalline composite compact. Home-made SPS equipment working at 24 V and 3.75 kA was used. Also, the current pulse has a rectangular shape. On heating, the pulse ON-time was 20 ms, and OFF-time was 20 ms. Sintering parameters used for as-obtained sintered compacts were temperature ranging from 750 to 900^{o}C, sintering time - 0 min. (without holding time), the pressure applied during sintering was 30 MPa and sintering atmosphere was Ar. The sintering temperature was measured at 2 mm from sample with a thermocouple inserted in graphite mold. The particle sizes distribution has been determined using a Laser Particle Sizer (Analysette 22 NanoTec -

Fritsch), by wet dispersion technique (water – dispersion liquid), with an analysis field of 10 nm to 1000 μm. For the X-ray diffraction studies an Inel Equinox 3000 diffractometer with Co radiation ($\lambda_{Co\ Ka}$ = 0.1790300 nm) equipped with a high-temperature chamber-Anton Paar HTK 1200 N was used. The diffraction patterns were recorded in the angular range 2θ = 30-110°. For HT-XRD in situ analyses, the heating rate was 10°C/min. up to 900°C. The mean crystallite sizes were computed using Scherrer method [30]. A JEOL-JSM 5600 LV scanning electron microscope (SEM) coupled with an energy-dispersive X-ray (EDX) spectrometer (Oxford Instruments, INCA 200 software) was used for the investigation of particles morphology and local chemical homogeneity.

3. Results and Discussion

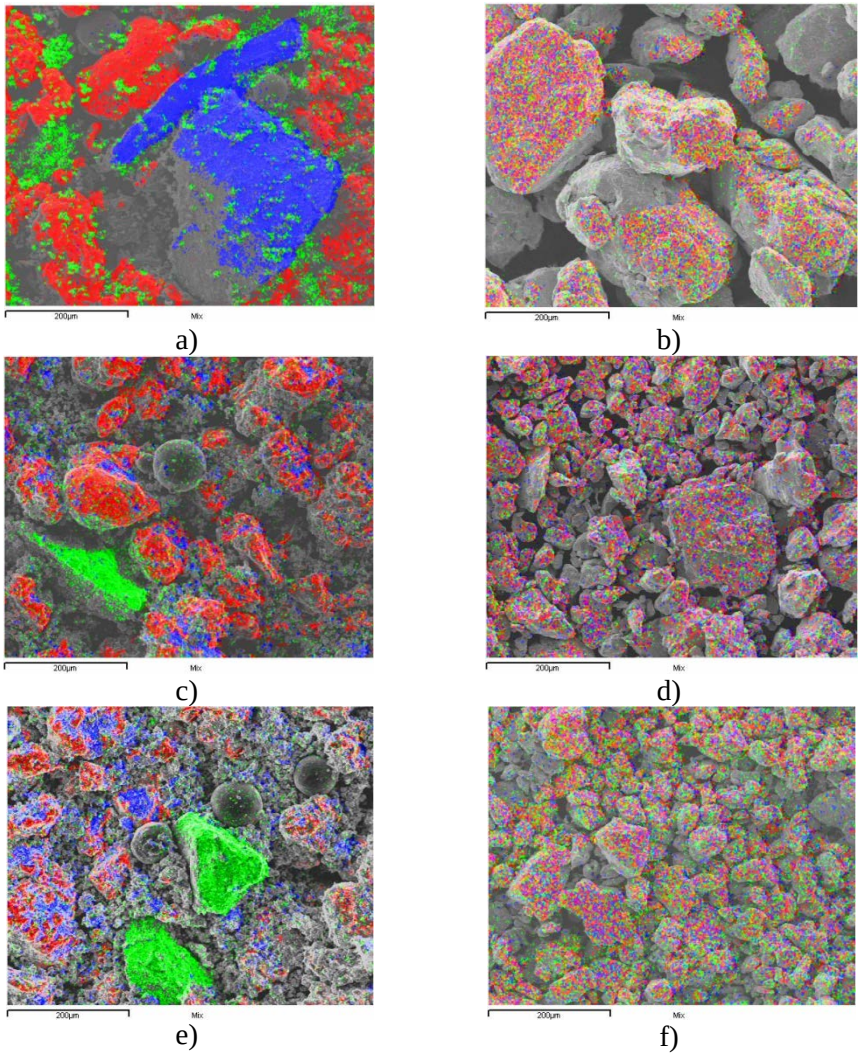

Fig.1. SEM images and elemental map distribution of Superalloy and Superalloy/Al_2O_3 powders: a – unmilled Superalloy powders (starting sample); b – Superalloy powders milled up to 16 h; c – Superalloy/5 % Al_2O_3 powders (starting sample); d - Superalloy/5 % Al_2O_3 powders milled up to 16 h; e - Superalloy/10 % Al_2O_3 powders (starting sample) and f - Superalloy/10 % Al_2O_3 powders milled up to 16 h.

In Fig. 1 are shown the SEM-EDX images of both superalloy and superalloy/Al_2O_3 powders unmilled and after milling up to 16 h. It can be observed spherical particles, which is Ti powder, Fe powders - large irregular shape particles (red colour), Cr powders – flat particles (blue colour) and Ni powders - the smallest particles (green colour) (Fig. 1a). In added, in Fig. 1c and e it can be seen the Al_2O_3 particles – small agglomeration (blue). After 16 h of milling, on the base of SEM images, we can conclude that the superalloy powders are larger than the superalloy/Al_2O_3 powders. The particles are also flattened, and their shape is irregular with rounded edges (Fig. 1b). With the increase of Al_2O_3 powder content, the particle sizes decrease (Fig. 1d and f). The particle has an irregular polyhedral shape. The elemental map distributions (EDX) are overlapped with the SEM images.

Particle sizes distribution of starting mixture formed by elemental powders (superalloy and superalloy/Al_2O_3) are shown in Fig. 2. All the curves present a multimodal distribution of particle sizes. The particle size distribution of powder mixtures with different densities is difficult to analyze by wet dispersion laser scattering. However, according to the particle size distribution curves, presented in the fig 2, it can be observed the increase of the amount of the fine particles (size ranges 0.2-4 μm and 4-20 μm) together with the increase of the amount of alumina (from 5 to 10 %vol).

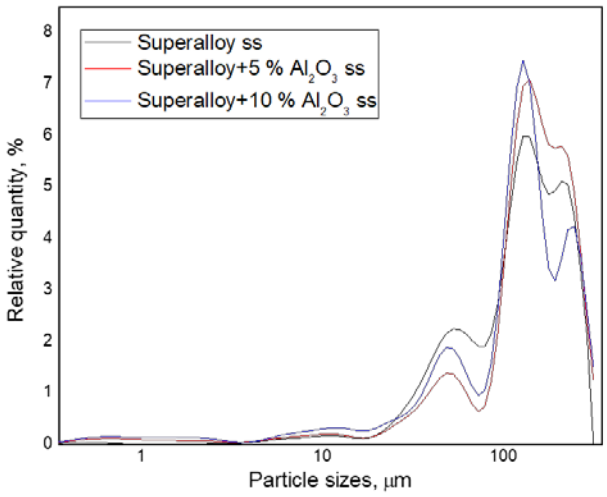

Fig. 2. Particle sizes distribution of starting samples.

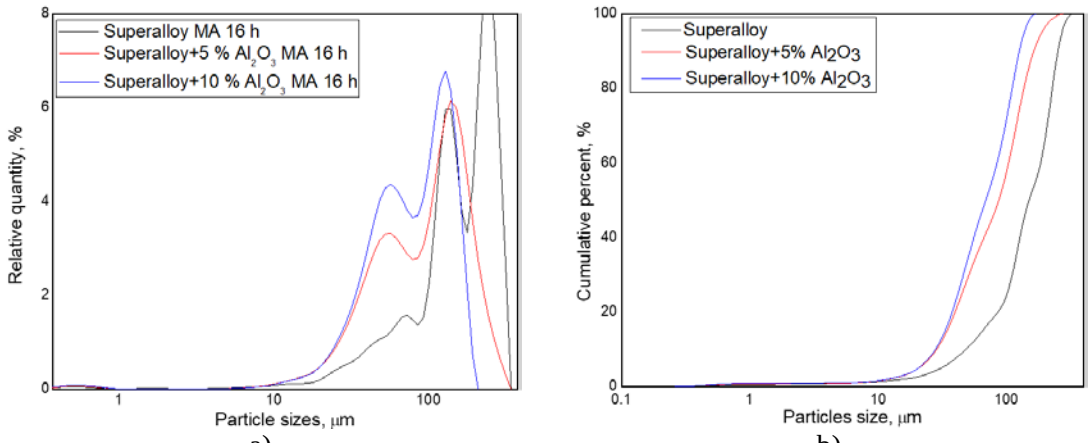

a) b)

Fig. 3. Particle size distributions of powders milled up to 16 h:
a) frequency distribution, b) cumulative curve.

In table III are shown the values of D_{10}, D_{50} and D_{90} corresponding to the superalloy and composite powders 16 h milled.

Tab. III Values of D_{10}, D_{50} and D_{90} corresponding to the superalloy and composite powders 16 h milled.

	Superalloy	**Superalloy +5 %vol. Al_2O_3**	**Superalloy +10 %vol. Al_2O_3**
D_{90} [µm]	263	171	132
D_{50} [µm]	157	90	72
D_{10} [µm]	50	30	29

Comparing the results of the particle size distribution analysis, for the starting mixture and for the mechanically alloyed powder after 16 h of milling (Fig. 2 and 3), a decrease of the fine fraction, smaller than ~ 20 µm can be observed. This may be due to the embedding of Al_2O_3 into the metal particles during mechanical alloying. Increasing the content of Al_2O_3 powder also influences the fragmentation mechanism during mechanical alloying, hindering the cold-welding processes. Higher aluminum oxide content (10 %vol. Al_2O_3) facilitates a µnarrower distribution of powder particles and decreases powder particles' size. This can be seen more clearly from Fig. 3b and Table III, the D_{90} values for each type of the powder mixture: 263 µm for superalloy powder, 171 µm for superalloy with 5 vol.% Al_2O_3 and respectively 132 µm for superalloy with 10 vol.% Al_2O_3.

In Fig. 4 are shown the X-ray diffraction patterns of superalloy powders milled up to 16 h. The Bragg characteristic peaks of Fe, Cr (BCC lattice) and Ni (FCC lattice) elemental powder has been identified in the pattern of start samples (ss). The maxima of Ti (HC lattice) and B (rhombohedral lattice) cannot be highlighted due the smaller amount in which these elements are presents (below of detection limit of the diffractometer). With milling time increasing, up to 4 h, only the broadening of the peaks occurs. A peak broadening is produced by internal stresses and microstructure refinement induces by mechanical milling. After 8 hours of milling it can be observed that the FCC characteristic peaks positions are shifted at lower angles. These are associated with increasing of the FCC crystal parameter due to the diffusion of the Cr and Fe in Ni matrix. The intensity of the peaks corresponding to BCC phases decreases, and the intensity of the FCC phases increases. At 16 h of milling, only the peaks of the FCC phase can be observed in the diffraction pattern.

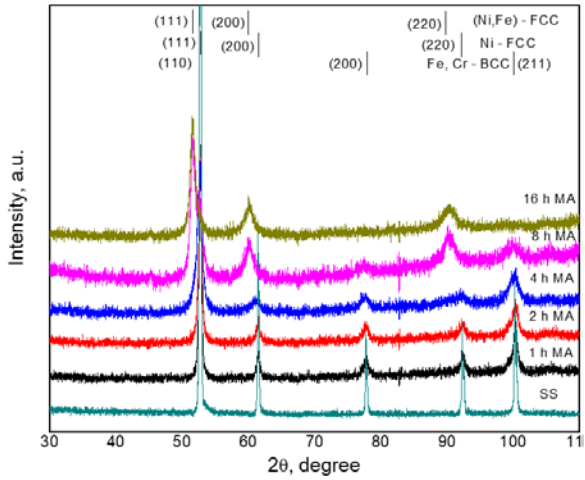

Fig. 4. X-ray diffraction patterns of superalloy powders milled up to 16 h.

Fig. 5 shows the X-ray diffraction pattern of superalloy/5 %vol. Al_2O_3 composite powders. In pattern of starting mixture, it can be identifier both the characteristic Bragg lines

of the elemental metallic powders (Fe, Ni and Cr) and of the ceramic component – Al_2O_3. Since the Al_2O_3 is the hard and brittle component, during the milling process it is fractured and is embedded in the ductile component, which is the metallic component – Fe, Ni and Cr. For this reason, in the first hours of milling, the diffraction peaks correspond to Al_2O_3 totally disappears. After 4 h of milling an asymmetry of the (100) peak of BCC phases can be observed and the (111) peak of FCC phase appear. At 8 hours of milling FCC phase is more visible due to the diffusion of Fe and Cr atoms in Ni FCC matrix. After 16 h of milling the FCC phase is prevalent. Moreover, the asymmetry of the (111) peak indicated that the FCC solid solution is not fully formed in the entire volume of milled powders.

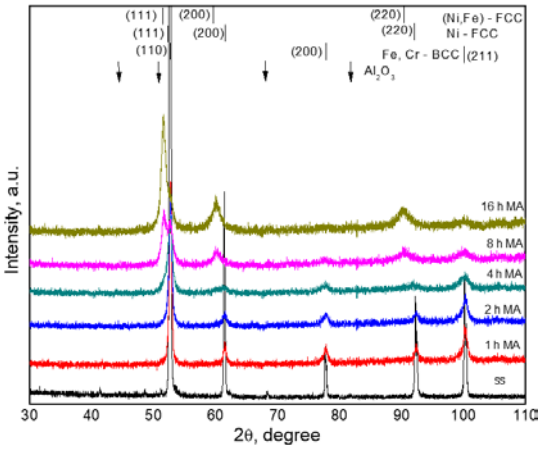

Fig. 5. X-ray diffraction pattern of superalloy/5 % Al_2O_3 powders milled up to 16 h.

In Fig. 6 are shown the XRD pattern of the superalloy with 10 vol.% Al_2O_3 powders. It can be observed that the peaks that correspond to Al_2O_3 no longer exist in diffraction pattern after 2 h of milling. The characteristic peaks of FCC phase are present in XRD pattern after 4 h of milling. With milling time increasing the characteristic peaks of FCC phase increase. Also, the peaks intensity of BCC phase decrease; after 16 h of milling only a small quantity of BCC phase remains in superalloy matrix. From above, also it can be concluded that the BCC phase amount is higher when the Al_2O_3 content increase due to the alumina particles hindering the atomic diffusion. To investigate the Al_2O_3 particle influence on superalloy's thermal stability, the mechanically alloyed powders were subjected to in situ HT-XRD analyses up to 900^{o}C.

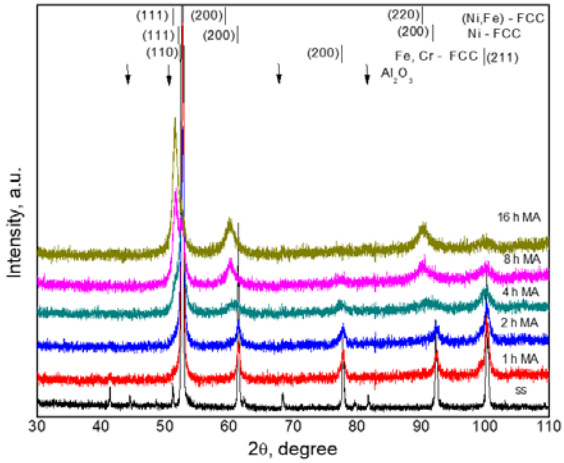

Fig. 6. X-ray diffraction pattern of superalloy/10 % Al_2O_3 powders milled up to 16 h.

The HT-XRD patterns of superalloy mechanically alloyed powder are shows in Fig. 7. With the increase of the temperature, only the narrowing of the diffraction peaks corresponding to the FCC phase occurs. This phenomenon is associated with both reducing the crystallites size due to recrystallization and internal stress removing.

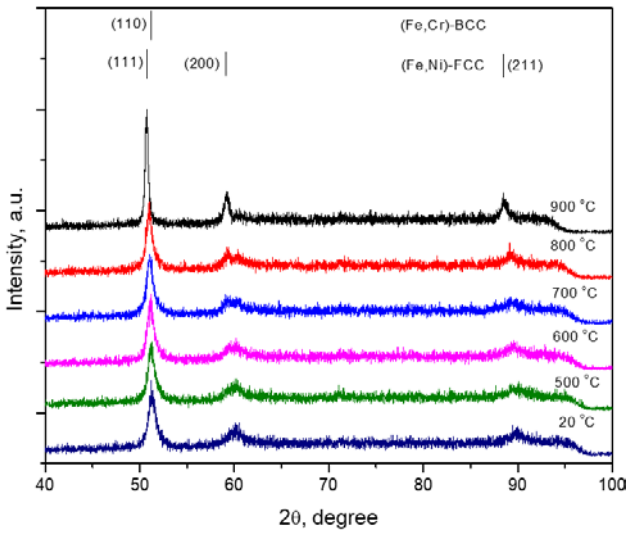

Fig. 7. HT-XRD patterns of mechanically alloyed superalloy powders.

Fig. 8 shows the HT-XRD patterns of superalloy/5 vol.% Al_2O_3 composite powders. It can be noticed that the two phases (BCC and FCC) are present in diffraction patterns up to 500°C. Also, the BCC phase characteristic peak is more visible with temperature increasing, up to 500°C, due to removal of internal stress. With temperature increase at around 600°C the BCC to FCC phase transition occurs. Thus, in the range of temperature between 600 to 900°C, only the FCC phase peaks can be identified in diffraction patterns.

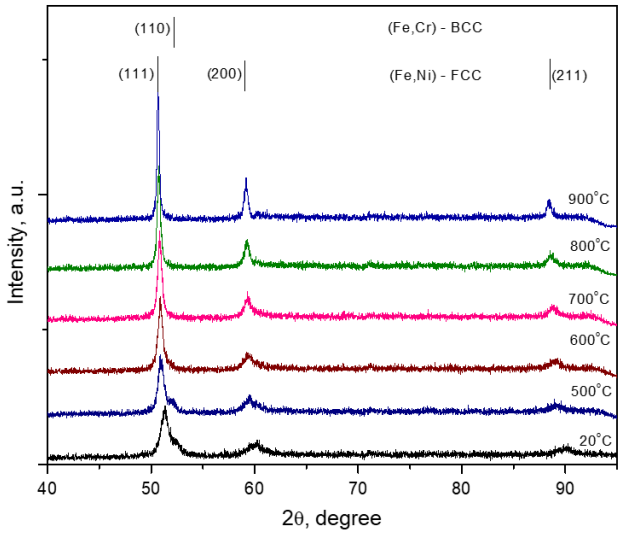

Fig. 8. HT-XRD patterns of mechanically alloyed superalloy/5 % Al_2O_3 composite powders.

The HT-XRD diffraction patterns of superalloy/10% Al_2O_3 composite (Fig. 9) show that the increasing of Al_2O_3 content leads to increase of both the BCC phase peak intensity and transition temperature at 700°C.

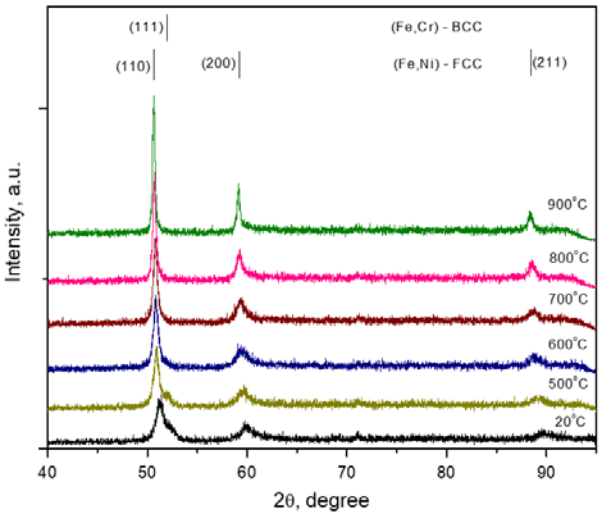

Fig. 9. HT-XRD patterns of mechanically alloyed superalloy/10 % Al_2O_3 composite powders.

From the above results, we can conclude that the BCC phase is present in a large quantity and is more stable with increasing of the alumina content. Due to the fragility of alumina, during the milling process, the fragmentation predominates. The fine alumina particles are enveloped by the metal powder particles, thus preventing the diffusion of Ni into Fe and the formation of the γ phase. Therefore, the alumina stabilizes the BCC phase. The evolution of the lattice parameter with temperature is shown in Fig. 10. It can be noticed that the lattice parameters of both phases, which crystallizes into a network bcc (superalloy with 5 and 10 % Al_2O_3) show an insignificant increase up to 200°C. In the range of 200 to 500°C, the lattice parameters increase with temperature increasing. The lattice parameters of the superalloy γ phase grow almost evenly and proportionally with the temperature increasing. In the case of the composite powders (superalloy with 5 and 10 % Al_2O_3), a sudden increase of lattice parameters of γ phases at 500°C can be attributed to the α-γ transition.

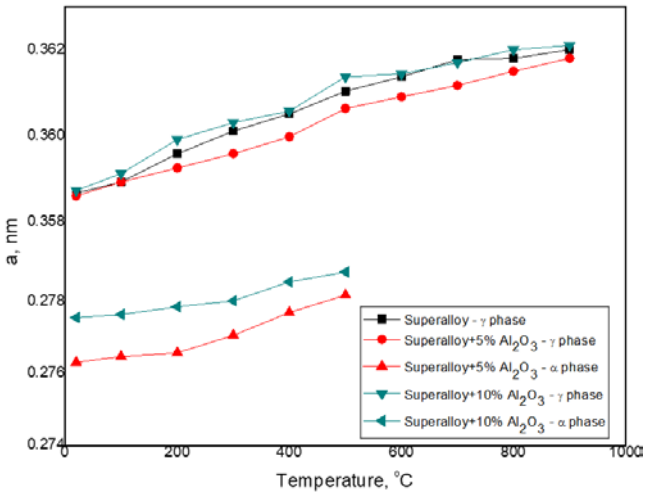

Fig. 10. Lattice parameter evolution versus temperature.

Using superalloy powders and superalloy with 5 and 10 vol.% Al_2O_3 composite powders were made compacts by SPS technique at 750 and 900°C. Fig. 11 shows the SEM image and the elemental distribution map (EDX) of superalloy compacts obtained by SPS at

900°C. It can be observed that the sample is homogeneous and consists of a single phase (Fig. 11a). The distribution maps (Fig. 11b) show that the metallic elements (Fe – red color, Ni – green color and Cr – yellow color) are evenly distributed.

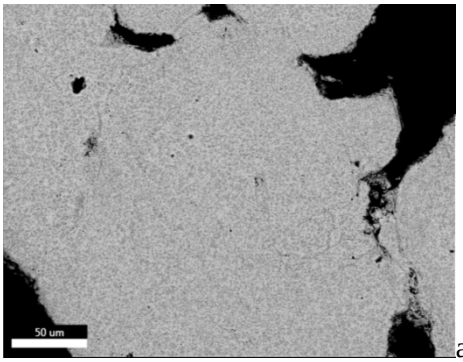

a)

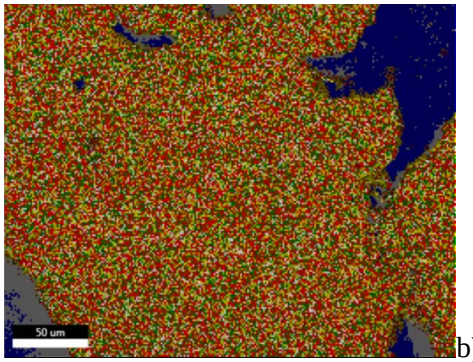

b)

Fig. 11. SEM image a) and the elemental distribution map (EDX) b) of superalloy compacts obtained by SPS at 900°C.

In Fig. 12 are shown the SEM images (a) and EDX analyzes (b) of superalloy/5 vol.% Al_2O_3 composite compact after sintering by SPS at 900°C. The Al_2O_3 (green color) relatively large particles (2-10 μm) are distributed at the boundary of the former superalloy particles. Also, it can be observed that the elements distribution is not uniform. The Cr rich phases (light brown color) can be identified.

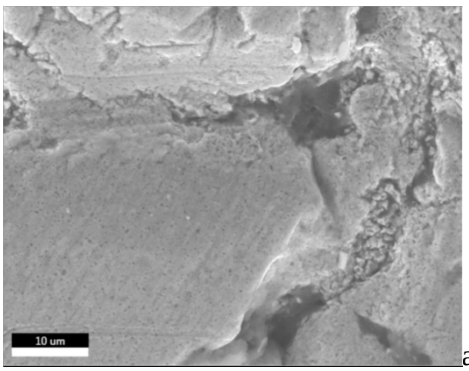

a)

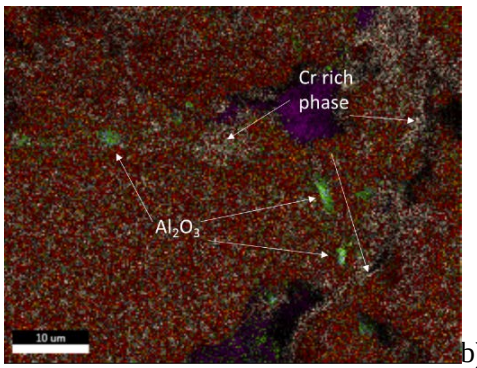

b)

Fig. 12. SEM image a) and EDX analyze b) of superalloy/5 % Al_2O_3 composite compact after sintering by SPS at 900°C.

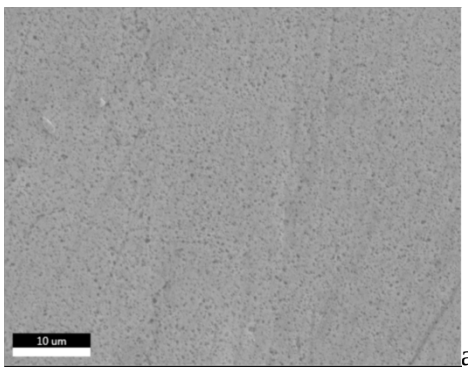

a)

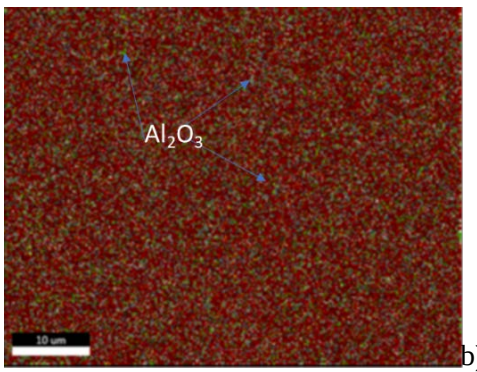

b)

Fig. 13. SEM image a) and elemental map distribution b) of superalloy/10 % Al_2O_3 composite compact sintered at 900°C.

The SEM image and elemental map distribution of superalloy/10 % Al_2O_3 composite compact sintered at 900°C is shows in Fig. 13. In SEM image (Fig. 13a.) it can be observed the homogenous structure of superalloy/10 % Al_2O_3 composite compact. The map distribution of elements (Fig. 13b.) shows that the Al_2O_3 particles (green color) are small (< 1 μm) and evenly distributed in the metallic matrix (Fe – red color, Ni – yellow color, Cr – light brown color) of the composite compact.

The compacts obtained by SPS technique after different sintering temperatures were subjected to XRD analyses (Fig. 14). In all diffraction patterns only the characteristics Bragg peaks of the FCC phase are identified. Also, it can be observed that the peaks width decreases with sintering temperature increasing due to the removal of internal stress accumulated during mechanical alloying process and recrystallization.

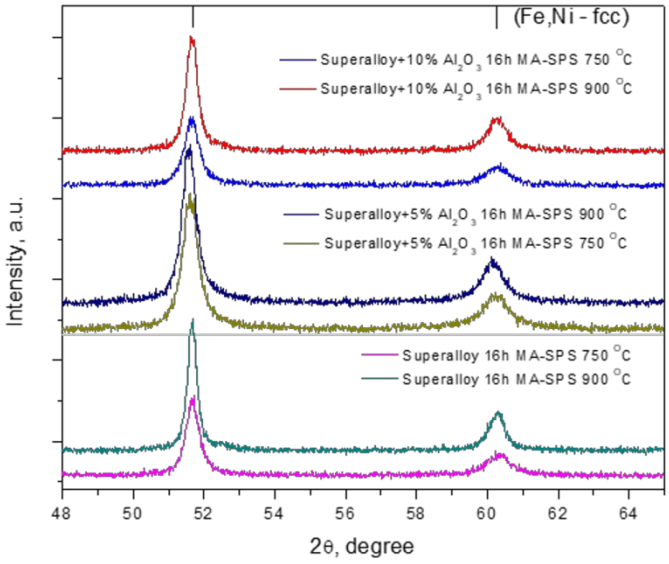

Fig. 14. XRD patterns of Superalloy compacts and composite superalloy compacts with 5 % and 10 % Al_2O_3 obtained by SPS at 750 and 900°C.

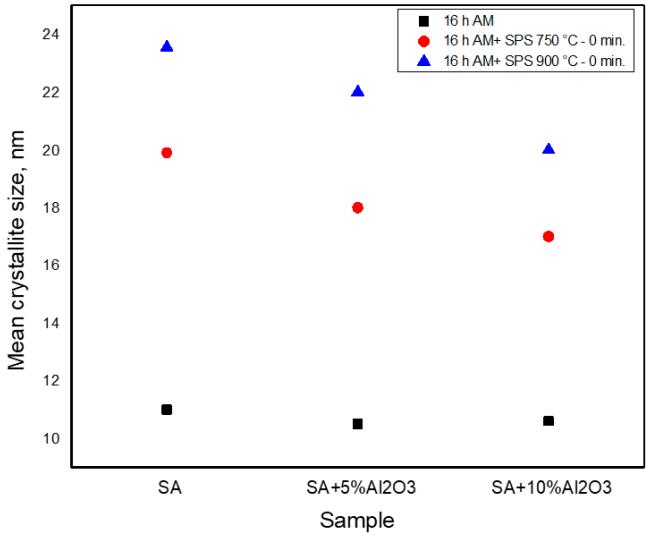

Fig. 15. Mean crystallite sizes of compacts obtained from superalloy and superalloy with 5 and 10 % Al_2O_3 composite powders by sintering at 750 and 900°C.

The mean crystallite sizes of compacts obtained by superalloy and superalloy with 5 and 10 vol.% Al_2O_3 composite powders by sintering at 750 and 900^oC are shown in Fig. 15. For comparison the mean crystallite sizes of powders milled up to 16 hours is also shown in Fig. 15. The values of crystallite sizes of superalloy and composite powders after 16 h of milling are almost the same (around 11 nm). After SPS, the values of the mean crystallite sizes increase with increasing sintering temperature. For the same sintering temperature, the value of crystalline sizes decreases with increasing Al_2O_3 content. Thus, the value of the mean crystallite size of superalloy compacts sintered at 750^oC increases from 19.5 nm to 23.7 nm in the case of sintering at 900^oC. With increasing the Al_2O_3 content, the average crystallite sizes of superalloy/5 vol.% Al_2O_3 composite compacts sintered at 750^oC degrease from 18 nm to 16.8 nm for superalloy/10 vol.% Al_2O_3 sintered at the same temperature. Also, if the sintering temperature used was 900^oC, the values of composite compacts crystallite sizes decreased from 22 nm to 20 nm if the Al_2O_3 content increased from 5 to 10 %.

From above results, it can be concluded that the Al_2O_3 particles, being evenly distributed in the particles, most probably in the crystallite's boundary by mechanical milling, it prevents diffusion and thus the growth of crystallites.

4. Conclusion

The superalloy composite compacts were successfully obtained by SPS technique from mechanically alloyed powders. The particle sizes of powders 16 h milled decrease with Al_2O_3 content increasing.

From XRD of both superalloy and superalloy/Al_2O_3 powders, it can be concluded the following: the lattice structure of superalloy powders milled for 16 hours are FCC; the BCC phase is present in superalloy with 5 vol.% and 10 vol.% Al_2O_3.

The HT-XRD diffraction patterns of superalloy and both composite powders (superalloy/5 vol.% Al_2O_3 and superalloy/10 vol.% Al_2O_3) show that the superalloy maintain its lattice (FCC) up to 900^oC , the BCC phase is stable in superalloy with 5 vol.% Al_2O_3 up to 600^oC and up to 700^oC in the case of superalloy/10 vol.% Al_2O_3 composites powder. Above these temperatures, the transition of BCC to FCC phase occurs.

The compacts obtain by SPS sintered at 750 and 900^oC from superalloy and composite powders have only FCC structure. The Al_2O_3 particle sizes from composite compacts sintered by SPS at 900^oC decrease with Al_2O_3 content increasing. Also, the crystallite sizes of compacts decrease with Al_2O_3 content increasing and increase with sintering temperature increasing.

5. References

1. L. Lin, Z. Jun, A. Cheng, Nickel-Based Superalloys, Encyclopedia of Materials: Metals and Alloys, 1 (2020) 294-304.
2. T. M. Pollock, S. Tin, J. Propuls. Power, 22 (2006) 361.
3. C. Y. Cui, Y. F. Gu, Y. Yuan, T. Osada, H. Harada, Mater. Sci. Eng., A, 528 (2011) 5465.
4. J. Yu, S. Guo, Y. Chen, J. Han, Y. Lu, Q. Jiang, C. Wang, X. Liu, Intermetallics, 110 (2019) 106466.
5. S. Gabel, S. Giese, B. Merle, I. Sprenger, M. Heilmaier,S. Neumeier, E. Bitzek, M. Göken, Adv. Eng. Mater., (2021) 2001464
6. V. J. Gobbi, S. J. Gobbi, D. A. Pereira Reis, J. L. A. Ferreira, J. A. Araújo, C. R. Moreira da Silva, Metals, 8 (2018) 877.

7. A. J. Mueller, R. Bianco, R. W. Buckman, Int. J. Refract. Met. Hard Mater., 18 (2000) 205.
8. D. M. Elzey, E. Arzt, Oxide Dispersion Strengthened Superalloys: The Role of Grain Structure and Dispersion During High Temperature Low Cycle Fatigue, Superalloys 1988 Edited by S. Reichman, D.N. Duhl, G. Maurer, S. Antolovich and C. Lund The Metallurgical Society, 1988.
9. F. Akhtar, Can. Metall. Q., 53 (2014) 253.
10. A. Macke, B. F. Schultz, P. Rohatgi, Adv Mater Process, (2012) 19.
11. H. Wang, D. Zuo, Y. Sun, F. Xu, D. Zhang, Trans**.** Nonferrous Met. Soc. China, 19 (2009) 586.
12. K. R. Ramkumar, S. Ilangovan, S. Sivasankaran, A. S. Alaboodi, J. Alloys Compd., 688 (2016) 518.
13. W. Man, S. Hongying, Z. Lei, Z. Guangming, L. Shaofu, Z. Zhangjian, Powder Technol., 272 (2015) 309.
14. U. Martin, M. Heilmaier, Adv. Eng. Mater, 6 (2004) 515.
15. H. Hadraba, R. Husák, I. Kuběna, R. Bureš, M. Fáberová, M. Strečková, Powder Metall. Prog., 14 (2014) 222.
16. K. Dash, B. C. Ray, D. Chaira, J. Alloys Compd., 516 (2012) 78.
17. M. Mounib, M. Pavese, C. Badini, W. Lefebvre, Dieringa H., Adv Mater Sci Eng., (2014) 1.
18. Dinesh Kumar Koli, Geeta Agnihotri, Rajesh Purohit, Int J Latest Trends Eng Tech, 2 (2013) 486.
19. B. Prabhu, C. Suryanarayana, An L., Vaidyanathan R., Mater. Sci. Eng. A, 425 (2006) 192.
20. C. V. Pricǎ, B. V. Neamţu, F. Popa, T.F. Marinca, N. Sechel, I. Chicinaş, J. Mater Sci, 53 (2018) 3735.
21. E. A. Olevsky, D. V. Dudina, Field-Assisted Sintering: Science and Applications, Springer International Publishing, Cham, Switzerland (2018).
22. P. Cavaliere (Ed.), Spark Plasma Sintering of Materials: Advances in Processing and Applications, Springer International Publishing, Cham, Switzerland (2019).
23. M. I. Makena, M. B. Shongwe, M. M. Ramakokovhu, P. A. Olubambi, J. Alloys Compd., 699 (2017) 1166.
24. N. Sharma, S. N. Alam, B. C. Ray, Fundamentals of Spark Plasma Sintering (SPS): An Ideal Processing Technique for Fabrication of Metal Matrix Nanocomposites. In: Cavaliere P. (eds) Spark Plasma Sintering of Materials. Springer, 2019.
25. Mamoru Omori, Mat Sci Eng A, 287 (2000) 183.
26. Z. A. Munir, D. V. Quach, M. Ohyanagi, J. Am. Ceram. Soc., 94 (2011) 1.
27. M. K. Khouzani, A. Bahrami, M. Y. Mehr, J. Alloys Compd., 782 (2019) 461.
28. Y. Bai, R. Zhang, Y. Qi, C. Cui, Y. Cai, Vacuum, 186 (2021) 110033.
29. C. Voicu, F. Popa, T. F. Marinca, B. V. Neamtu, M. Lostun, N. Lupu, I. Chicinaş, Powder Metall., 61 (2018) 251.
30. P. Scherrer, Nachrichten Gesellschaft Wissenschaft Gottingen, 2 (1918) 98.

Сажетак: *Композити типа Al_2O_3 и суперлегуре на бази гвожђа су успешно синтетисани из механички легираних прахова синтерованих у плазми. Прах суперлегуре без Al_2O_3 и суперлегуре/Al_2O_3 типа композита са 5 и 10 % vol. Al_2O_3 су синтетисани из елементарних прахова у високо-енергетском планетарном млину. Утицај процеса млевења на расподелу величине честица је одређен употребом Laser Particle Size Analyzer у рангу 0.1-1000 μm. Узорци композита су добијени синтеровањем*

у плазми. И прахови и синтеровани узорци су испитивани уз помоћ XRD, HT-XRD, SEM и EDX методама.
***Кључне речи**: суперлегура/Al_2O_3 композит, механичко легирање, синтеровање у плазми.*